Monthly Notices
of the
ROYAL ASTRONOMICAL SOCIETY

Mon. Not. R. Astron. Soc. **412,** 1611–1626 (2011) doi:10.1111/j.1365-2966.2010.17999.x

Diagnostic tool to analyse colour–magnitude diagrams of poorly populated stellar concentrations

D. B. Pavani,[1⋆] L. O. Kerber,[2] E. Bica[1] and W. J. Maciel[3]

[1] *Universidade Federal do Rio Grande do Sul, IF, CP 15051, Porto Alegre 91501-970, RS, Brasil*
[2] *Universidade Estadual de Santa Cruz, 45662-000, Campus Soane Nazaré de Andrade, km16, Rodovia Ilhéus-Itabuna, Ilhéus, BA, Brazil*
[3] *Universidade de São Paulo, IAG, Rua do Matão 1226, Cidade Universitária, São Paulo 05508900, SP, Brazil*

Accepted 2010 November 8. Received 2010 November 7; in original form 2010 August 17

ABSTRACT

The dynamical processes that lead to open cluster disruption cause its mass to decrease. To investigate such processes from the observational point of view, it is important to identify open cluster remnants (OCRs), which are intrinsically poorly populated. Due to their nature, distinguishing them from field star fluctuations is still an unresolved issue. In this work, we developed a statistical diagnostic tool to distinguish poorly populated star concentrations from background field fluctuations. We use 2MASS photometry to explore one of the conditions required for a stellar group to be a physical group: to produce distinct sequences in a colour–magnitude diagram (CMD). We use automated tools to (i) derive the limiting radius; (ii) decontaminate the field and assign membership probabilities; (iii) fit isochrones; and (iv) compare object and field CMDs, considering the isochrone solution, in order to verify the similarity. If the object cannot be statistically considered as a field fluctuation, we derive its probable age, distance modulus, reddening and uncertainties in a self-consistent way. As a test, we apply the tool to open clusters and comparison fields. Finally, we study the OCR candidates DoDz 6, NGC 272, ESO 435 SC48 and ESO 325 SC15. The tool is optimized to treat these low-statistic objects and to separate the best OCR candidates for studies on kinematics and chemical composition. The study of the possible OCRs will certainly provide a deep understanding of OCR properties and constraints for theoretical models, including insights into the evolution of open clusters and dissolution rates.

Key words: methods: data analysis – methods: statistical – open clusters and associations: individual: DoDz 6 – open clusters and associations: individual: NGC 272 – open clusters and associations: individual: ESO 435 SC48 – open clusters and associations: individual: ESO 325 SC15.

1 INTRODUCTION

In recent years, several authors have developed algorithms with a view to optmize and automatize the analyses of colour–magnitude diagrams (CMDs) and structure of open clusters (e.g. Kharchenko et al. 2005; Bonatto & Bica 2007; Froebrich, Scholz & Raftery 2007; Monteiro et al. 2010) and for the Large Magellanic Cloud with the *HST* (e.g. Kerber & Santiago 2005) to face the flow of observations available now and in coming years. This study has similar aims for poorly populated stellar concentrations.

Open clusters are formed embedded in dense cores of molecular clouds in the Galactic disc. The interplay between the internal cluster properties and external conditions contributes to the cluster decrease of density and total mass. As a consequence, open cluster dissolution is unavoidable. Oort (1958) first pointed out the scarcity of open clusters older than 1.0 Gyr in the Galaxy, suggesting a dissolution time-scale of 500 Myr. Since then, theoretical (including *N*-body simulations) and observational studies have analysed the dynamical processes involved in dissolution times.

Since fossil remnants occur, how can late dynamical evolutionary stages be investigated? The objects to investigate are the open cluster remnants (OCRs) that can be defined as a poorly populated concentration of stars, with enough members to show evolutionary sequences in the CMD, as a result of the dynamical evolution of an initially more massive physical system (Pavani et al. 2001). OCRs are expected to contain a high binary fraction (de la Fuente Marcos 1997). For longer lifetimes, *N*-body simulations for open clusters show that the evolution of the mass function is dominated by low-mass star depletion (Kruijssen 2009). We can expect that poorly populated star concentrations that may represent possible physical systems in more evolved dynamical states

⋆E-mail: dpavani@if.ufrgs.br

have this signature in their CMD star distribution (Davenport & Sandquist 2010).

Bica et al. (2001) presented 34 possible OCRs (POCRs) that are underpopulated with respect to usual open clusters at $|b| > 15^\circ$. The objects show a significant density contrast of brighter stars as compared to the Galactic field. Our group has studied objects from that list. NGC 1901 and 1252 were concluded to be OCRs (Pavani et al. 2001). We employed *B*, *V* photometry, proper motions from Tycho-2 and comparisons of object CMDs with model predictions for the Galactic field. Ruprecht 3 was studied with 2MASS photometry (Skrutskie et al. 2006) and integrated spectroscopy, and was concluded to be an OCR (Pavani et al. 2003). In Pavani & Bica (2007), 18 POCRs were tested against the surrounding fields by means of statistical CMD comparisons using 2MASS photometry. Subsequently, eye-fit isochrones provided OCR fundamental parameters. Limiting radii were obtained from the stellar density profiles. The methods indicate 12 OCRs and six field stellar fluctuations. Based on those approaches, we provide in this work further methods of improvement.

Any physical stellar group must (i) occupy a limited volume of space; (ii) share a common space velocity, age and chemical composition; and (iii) produce distinctive sequences in Hertzsprung–Russell diagrams (Platais, Kozhurina-Platais & van Leeuwen 1998). Photometry is the main information available for POCRs. The 2MASS data base provides objects and fields homogeneously together with photometric errors and completeness estimates. The main purpose of this paper is to present a method that explores 2MASS photometric information using automated tools to detect objects that cannot be explained as field fluctuations. In order to disentangle poorly populated systems from the field, we use the 2MASS CMDs to statistically compare the former with the latter and to assign membership probabilities. By means of an isochrone fitting, we built an objective criterion to verify if the POCRs satisfy the Platais et al.'s condition (iii). The POCRs that satisfy this condition are the best candidates for studies of the stellar content to confirm, or not, them as physical systems. The present method optimizes the study of POCRs.

In Section 2, we present the objects. In Section 3, we use the dynamically evolved open cluster NGC 3680 and the dissolving open cluster NGC 2180 to explain the sequence of steps used to analyse each POCR, as well as to test the statistical method employed. In Section 4, the results are presented. Finally, the conclusions are given in Section 5.

2 THE SAMPLE

The POCRs were selected from open cluster catalogues and visual inspections in the Digitized Sky Survey (DSS)[1] maps. We employ amongst the available digitized images (DSS – *B* band or XDSS – *B, R* or *I* bands) the one that most clearly shows the object. Important factors are in general: (i) they are originated in more- or less-exposed plates; (ii) they might include nebular emission or reflexion; and (iii) reddening effects may demand the *R* or *I* band. The POCRs are located at relatively high Galactic latitudes ($|b| > 15^\circ$) and are underpopulated compared with usual open clusters.

The coordinates of the objects are given in Table 1. We also include the open clusters NGC 3680, NGC 2180 (Bonatto, Bica & Pavani 2004) and a Test Field for comparison purposes. By columns: (1) designation; (2) and (3) Galactic longitude and latitude, respectively; and (4) and (5) J2000.0 equatorial coordinates. We confirmed the equatorial coordinates using the maximum central stellar density contrast (Bonatto & Bica 2009b).

Table 1. Galactic and equatorial coordinates of POCRs and open clusters NGC 3680, NGC 2180 and Test Field.

Designation	ℓ (°)	b (°)	α (h m s)	δ (° ′ ″)
NGC 3680	286.76	16.92	11:25:38	−43:14:30
NGC 2180	203.85	−7.01	06:09:48	04:48:26
Test Field	200.97	20.02	7:44:19	19:13:51
DoDz 6	61.58	40.36	16:45:24	38:21:00
NGC 272	122.90	−27.02	0:51:18	35:50:51
ESO 435 SC48	264.81	22.28	10:09:35	−28:21:28
ESO 324 SC15	309.32	20.59	13:23:37	−41:52:55

We extracted *J* and *H* photometry from the 2MASS Catalogue by means of the Vizier Service.[2] The photometric uncertainties typically reach 0.1 mag at $J \approx 16.0$ and $H \approx 15.0$ (Soares & Bica 2002). The analysis of the 2MASS Catalogue[3] allows the estimate of completeness as a function of ℓ and b. Considering photometric uncertainties and completeness, as well as that the POCRs in this work have $|b| > 15^\circ$, the derived limits are $J < 15.8$ and $H < 15.1$ mag. As a photometric quality constraint, we extracted only stars with *J* and *H* errors lower than 0.15 mag.

For each object, we made a circular extraction centred in the coordinates given in Table 1. To analyse POCRs and fields, we used an angular extraction radius of 30 and a 2-arcmin ring area was considered to separate the object and field.

The intermediate-age open cluster NGC 3680 resembles in several aspects what is expected for OCRs, as discussed in Pavani & Bica (2007). In this work, we employ it again as a comparison object. The fundamental parameters of NGC 3680 are the age $\tau_{\rm age} = 1.6 \pm 0.01$ Gyr, distance of the Sun $d_\odot = 1.0$ kpc and a reddening value $E(B-V) = 0.0$. Bonatto et al. (2004) suggested NGC 2180 as a disrupting open cluster in a dynamical stage intermediate between an open cluster like NGC 3680 and OCRs. The fundamental parameters derived are $\tau_{\rm age} \approx 710$ Myr, $d_\odot = 0.9$ kpc and $E(B-V) = 0.0$. Kharchenko et al. (2005) also concluded it to be a physical system but with an older age $\tau_{\rm age} \approx 1.7$ Gyr. NGC 2180 presents an eroded extended density profile with a central concentration of stars for $R < 5$ arcmin and an excess in the corona at $14 \leq R \leq 18$ arcmin (fig. 4 of Bonatto et al. 2004). The Test Field was selected within the limits of the POCR sample latitude coordinates to represent the expected behaviour of the field star fluctuations. NGC 3680, NGC 2180 and Test Field underwent the same statistical treatment as the POCRs.

The previous literature data about the present POCR sample are scarce. NGC 272 is the only object included in the WEBDA data base (Mermilliod & Paunzen 2003),[4] but no fundamental parameters have been derived for it. DAML02 (Dias et al. 2002)[5] includes DoDz 6 as a POCR and ESO 435 SC48 as a dubious object (considering DSS images), while no classification is available for ESO 324 SC15.

[1] http://cadcwww.dao.nrc.ca/cadcbin/getdss

[2] Available at http://vizier.u-strasbg.fr/viz-bin/VizieR (Ochsenbein, Bauer & Marcout 2000).

[3] http://www.ipac.caltech.edu/2mass/releases/allsky/doc/sec6.html

[4] http://obswww.unige.ch/webda

[5] http://www.astro.iag.usp.br/∼wilton/

3 DIAGNOSTIC TOOL

Automated methods have been applied in the search of open and embedded clusters. Reylé & Robin (2002) employed stellar densities and the integrated K_s-band flux. Ivanov et al. (2002) used the K_s luminosity function and the distribution of stars in $J - K_s$. Statistical methods are employed to identify overdensities as possible star clusters (Mercer et al. 2005; Froebrich et al. 2007). Kharchenko et al. (2005) presented astrophysical parameters of open clusters, where more probable main-sequence stars are identified kinematically, and fundamental parameters are determined by an automated CMD analysis. Bonatto & Bica (2007) decontaminated clusters projected on extremely dense background fields in the bulge and/or disc at low latitude. The methods above may not be suitable for POCRs because of their low star counts. Thus, an objective statistical method is required.

With this in mind we developed a diagnostic tool to analyse CMDs of POCRs to disentangle them from the field, and to derive age, distance and reddening in a self-consistent way. The method assigns to each POCR star a membership probability and by taking this probability into account, it finds a set of isochrone fits that maximize the number of fitted stars. Applying the same procedure for neighbouring field samples that are selected within a surrounding control field, the method tests whether or not the POCR can be understood as a field fluctuation. As an additional check, we inspect the set of field CMDs that the tool indicated as most resembling the object (Section 3.4).

The steps employed to analyse each POCR are explained in the following sections.

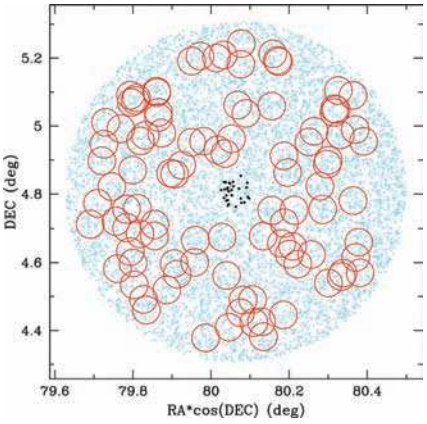

Figure 1. Example of neighbouring field samples randomly selected (circles) around NGC 2180. This plot presents the stars with $J < 15.8$ mag for $R < 30$ arcmin. In the central part are shown the stars within $R_{cut} = 3.0$ arcmin (dots).

3.1 Determining the cut-off radius

First, we determine a cut-off radius (R_{cut}) to select the number of stars (N_{POCR}) in the target. It corresponds to a rare count as compared with the surrounding control field. To compute this radius, we build the star-count distributions for the field (N_{field}). We use neighbouring field samples randomly selected from the background concentric zone that corresponds to the surrounding control field (Fig. 1). The number of comparison fields ($N_{samples,tot}$) depends on the ratio of the field to POCR areas. The minimum number is 100 for $R_{cut} >$ 3 arcmin and the maximum number is 896 for $R_{cut} = 2$ arcmin. The extraction radii are fixed (30 arcmin) and the POCR radii are variable.

To determine R_{cut} for each object, the angular radius of the neighbouring field samples is varied together with the target radius. The radii are varied from large to small values (9 to 1 arcmin for POCRs). Star countings are performed until a significant contrast between the target and field samples occurs. The computations are repeated 10 times to determine the fluctuation around each tested radius. In each iteration, new centres for the field samples are chosen randomly. The centres are kept fixed throughout the cut-off radius search. The resulting R_{cut} value will be the radius that maximizes the percentile position for $N_{POCR}/\langle N_{field}\rangle$ in the $N_{field}/\langle N_{field}\rangle$ distribution (Fig. 2). Objects below the 95th percentile are not distinguishable from field fluctuations and can be characterized as such.

The steps to determine R_{cut} are shown in Figs 2 and 3. They illustrate the search for R_{cut} and the final comparison between the number of stars for the object within a radius and that for the field star distribution. The present method is optimized to low counts and for this reason, we use for NGC 3680 $R_{cut} = 2R_{core} = 4.6$ arcmin (Bonatto et al. 2004). Comparing panels in Fig. 2, we can see the difference between an open cluster, the disrupting one NGC 2180 and the Test Field. Fig. 2 shows that for NGC 3680 the associated percentiles are above 99 per cent as far as $R \leq 8$ arcmin. The abrupt percentile decrease to 70th at 10 arcmin, followed by a peak at 85th in 15 arcmin, agrees well with the behaviour in the radial density profile shown in fig. 4 of Bonatto et al. (2004). For NGC 2180,

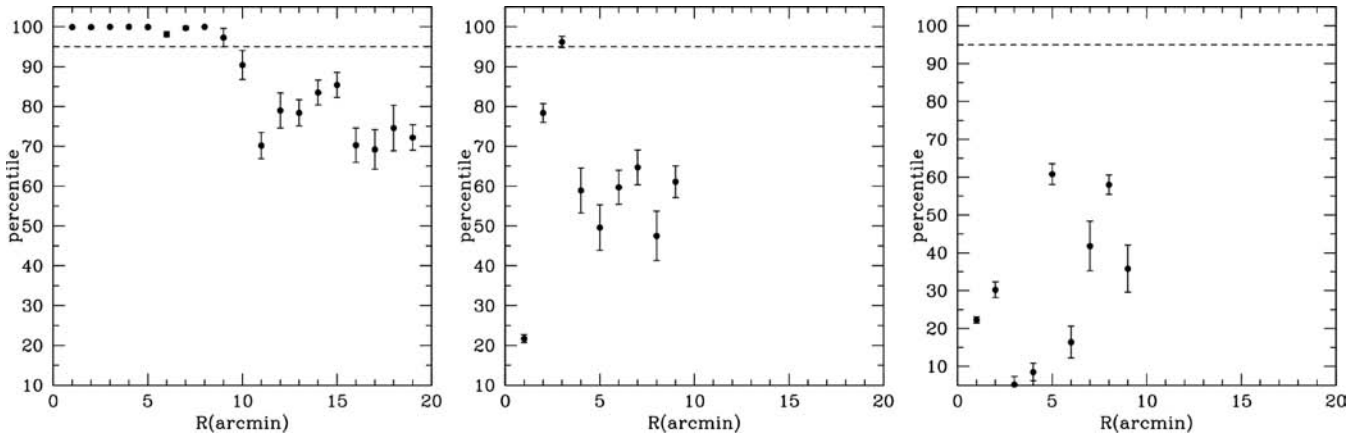

Figure 2. Examples for the search of the radius that maximizes the percentile position. For each radius is shown the associated percentile. The horizontal dashed line indicates the 95th percentile locus. Left-hand to right-hand panel: NGC 3680, NGC 2180 and Test Field.

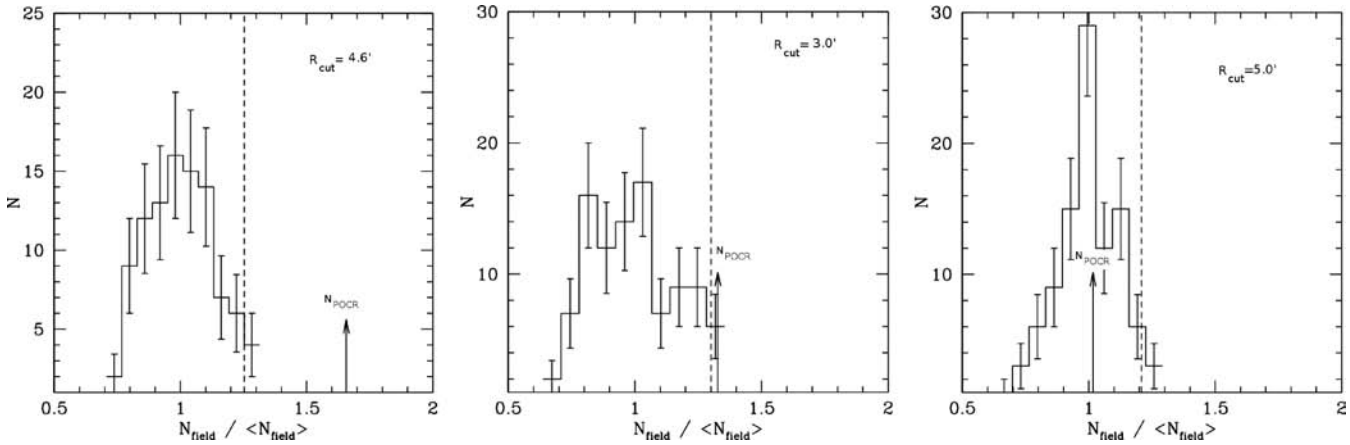

Figure 3. Examples of star count distributions for the field star samples compared to the same quantity for the targets $N_{\rm POCR}$ (arrow). Left-hand to right-hand panel: NGC 3680, NGC 2180 and Test Field. The 95th percentile locus is shown (vertical dashed line). $R_{\rm cut}$ values are indicated.

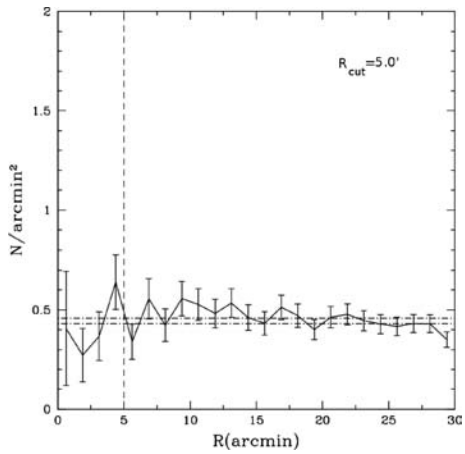

Figure 4. The Test Field radial stellar density distribution with the stellar field density averages (horizontal dashed line). $R_{\rm cut}$ is also shown (vertical dashed line).

Table 2. Number of observed stars within $R_{\rm cut}$.

Designation	$R_{\rm cut}$ (arcmin)	$\langle N_{\rm field}\rangle$	$\sigma_{N_{\rm field}}$	$N_{\rm POCR}$	$N_{\rm POCR,clean}$
NGC 3680	4.6	49.5	7.0	82	32.8
NGC 2180	3.0	37.2	5.9	29	10.5
Test Field[a]	5.0	36.4	4.7	37	5.64
DoDz 6[b]	3.0	7.2	2.3	14	9.4
NGC 272	3.0	9.5	3.2	15	8.2
ESO 435 SC48	2.0	5.4	2.3	12	9.0
ESO 324 SC15	2.0	8.0	2.6	17	12.0

[a]The $R_{\rm cut}$ maximum percentile position is 60 per cent.
[b]Results from solution 1.

$R_{\rm cut} = 3$ arcmin corresponds to the only value significantly above the 95th percentile. The Test Field does not present any radius above or equal to the percentile 95th and the radial stellar density distribution (Fig. 4) corresponds to the one expected for a field star fluctuation. Fig. 3 shows differences between NGC 3680, NGC 2180 and the Test Field. Their classifications can be estimated by means of the relative loci of $N_{\rm POCR}$ and the respective field star distribution of $N_{\rm field}/\langle N_{\rm field}\rangle$.

The $R_{\rm cut}$ determinations are given in Table 2. Column (1) gives the POCR or other object designation; column (2) gives $R_{\rm cut}$; columns (3) and (4) give the average ($\langle N_{\rm field}\rangle$) and standard deviation ($\sigma_{\rm field}$) for the star count in the neighbouring field samples, respectively; column (5) shows the number of stars in the POCR direction ($N_{\rm POCR}$); and column (6) gives the number of stars after field star decontamination ($N_{\rm POCR,clean}$) (Section 3.2).

3.2 Field star contamination

The field star contamination for POCRs is a critical point. To tackle this, we developed a statistical method to compute this contamination in the POCR sample. This method was basically inspired by the field star decontamination process presented by Mighell et al. (1996), Kerber et al. (2002) and Kerber & Santiago (2005). Although these works dealt with rich stellar clusters, we adapted their principle to the present case. Therefore, we assume a CMD of a surrounding control field as representative of the field and by a comparison with the POCR CMD, we compute the probability for any POCR star to belong to it. Therefore, for the *j*th POCR star, this membership probability is defined as

$$P_{{\rm POCR},j} = 1 - \frac{N_{\rm field,box}}{N_{\rm POCR,box}} \frac{\Omega_{\rm POCR}}{\Omega_{\rm field}}, \quad (1)$$

where $N_{\rm POCR,box}$ and $N_{\rm field,box}$ are the number of POCR and surrounding control field stars observed in a box of dimensions $3\sigma_J \times 3\sigma_{J-H}$ (photometric errors in J and $J-H$, respectively) centred on this star. A priori $\Omega_{\rm field}$ and $\Omega_{\rm POCR}$ correspond to the solid angles for the surrounding control field and POCR, respectively.

Finally, the expected number of POCR stars after the decontamination process is defined as

$$N_{\rm POCR,clean} = \sum_{j=1}^{N_{\rm POCR}} P_{{\rm POCR},j}\ . \quad (2)$$

The results are shown in the last column of Table 2.

In the process of field star decontamination, we recall that the field samples are randomly selected from the background concentric zone given by $R_{\rm cut} + 2$ arcmin < 30 arcmin. Note that $N_{\rm POCR,clean}$ corresponds to the number of stars in the POCR direction weighted by the probability of each star to belong to the POCR. This information can be verified in size code for the CMDs (Figs 5 and 6). No star is removed from the CMD.

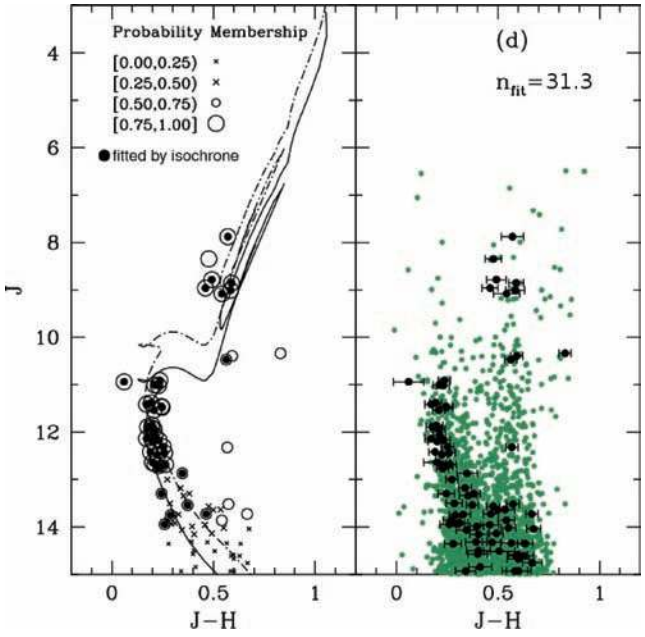

Figure 5. $J \times (J-H)$ CMD of NGC 3680. Left-hand panel: cluster stars within 4.6 arcmin are coded according to membership probability, solar metallicity, Padova isochrone (Girardi et al. 2002) of age, distance modulus and reddening $\log(\tau/\mathrm{yr}) = 9.11 \pm 0.04$, $(m-M)_0 = 10.34 \pm 0.22$, $E(B-V) = 0.02 \pm 0.01$. The shifted isochrone represents binaries of equal masses (dashed line). Filled circles indicate stars fitted by the isochrone by taking into account colour uncertainties. Right-hand panel: cluster stars within 4.6 arcmin (black dots) plotted over the stars in the field ($R = 30$ arcmin).

3.3 Searching for the best isochrone fits

To attribute a physical meaning to a POCR using its CMD, the first step is to find a set of best isochrone fits. We adopted a fixed solar metallicity, since clusters around the solar position in the disc have typically $-0.1 \leq [\mathrm{Fe/H}] \leq 0.0$ (Friel 1995). The depleted stellar content in POCRs does not provide enough constraints to discriminate metallicities with a method based on CMDs only. An objective way to look for these solutions is to define a parameter related to the quality of the fit. Thus, we define, for each proposed isochrone solution, the number of isochrone-fitted stars as

$$n_{\mathrm{fit}} = \sum_{j=1}^{N_{\mathrm{POCR,fit}}} P_{\mathrm{POCR},j}\ , \tag{3}$$

being the sum of probabilities $P_{\mathrm{POCR},j}$ computed only for the $N_{\mathrm{POCR,fit}}$ POCR stars that are at a maximum level of $2\sigma_J$ and $2\sigma_{J-H}$ from the nearest isochrone point. The effect of unresolved binaries is taken into account by shifting the isochrone by small steps up to 0.75 mag in J (corresponding to the sequence of binaries of equal masses) and adding the new fitted stars to $N_{\mathrm{POCR,fit}}$.

In general, the number of low-probability stars in POCR directions is greater than the high-probability ones. The former stars are generally fainter and have higher values of photometric uncertainties. To guarantee that these stars do not define the isochrone fit, the search for a set of best isochrone fits is restricted to stars with membership probability $\geq$50 per cent.

To test a suitable number of possible isochrone solutions, we first determine initial values for each physical parameter by eye [$\log(\tau)_{\mathrm{i}}$, $(m-M)_{0,\mathrm{i}}$ and $E(B-V)_{\mathrm{i}}$] and subsequently we investigate a large parameter space explored at equal steps. The isochrone solutions typically span the following physical ranges:

$$\log(\tau) = \log(\tau)_{\mathrm{i}} \pm 0.50, \tag{4}$$

$$(m-M)_0 = (m-M)_{0,\mathrm{i}} \pm 0.50, \tag{5}$$

$$E(B-V) = E(B-V)_{\mathrm{i}} \pm 0.10, \tag{6}$$

$$E(B-V) \leq E(B-V)_{\mathrm{S}} + 0.50, \tag{7}$$

where $E(B-V)_{\mathrm{S}}$ is the reddening value from Schlegel, Finkbeiner & Davis (1998). Thus, the only a priori constraints applied to the parameter space are related to reddening and metallicity. The steps for $\log(\tau)$, $(m-M)_0$ and $E(B-V)$ are 0.05, 0.05 and 0.01, respectively. Thus, for each POCR, we typically test 8000 isochrone solutions.

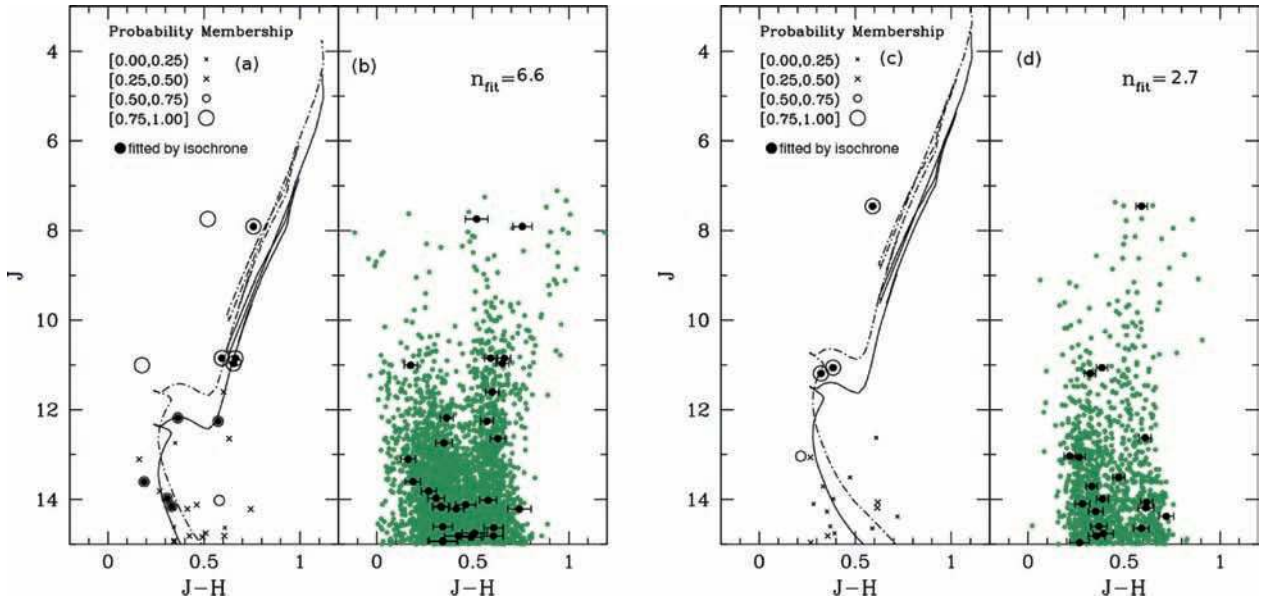

Figure 6. Same as Fig. 5, but for NGC 2180 in panels (a) and (b). Padova isochrone fit: $\log(\tau/\mathrm{yr}) = 9.20 \pm 0.3$, $(m-M)_0 = 11.4 \pm 0.6$, $E(B-V) = 0.21 \pm 0.1$. The Test Field corresponds to panels (c) and (d). A superposition of the isochrone is necessary to carry out the subsequent discussion.

The final values for the physical parameters of each cluster are defined as a set of isochrone solutions at the same quality level as the best one. Any solution that satisfies the criterion

$$n_{\rm fit} \geq n_{\rm fit,max} - 1.0 \quad (8)$$

is added to the set of best solutions, where $n_{\rm fit,max}$ is the maximum value found for $n_{\rm fit}$ for all tested isochrone solutions. Therefore, the new value (and uncertainty) for each physical parameter is defined as the average (and dispersion) for the best models. These average values are used as new guesses for a new iteration, until a variation of less than 5 per cent in the $n_{\rm fit,max}$ value is reached. Thus, we have the final parameter values, including the number of isochrone-fitted stars ($n_{\rm fit,POCR}$).

Fig. 5 presents the CMD of NGC 3680, where the isochrone fit stands for the average of the parameters for the best solutions. Each star in this panel is coded according to its $P_{\rm POCR}$ value and the stars fitted by the isochrone are indicated by filled circles. Only these stars are considered probable members. The surrounding field CMD of this open cluster is also shown. The CMDs are presented in Fig. 6 for NGC 2180 and the Test Field. The NGC 2180 CMD represents the expected behaviour for POCR CMDs: a small number of stars distributed along the evolutionary sequence. Particularly, we have the presence of giant stars. Although an isochrone fit is shown in the Test Field CMD, the distribution of stars does not represent the expected behaviour of an open cluster or POCR. The algorithm employs in the fits stars with membership probability ≥50 per cent.

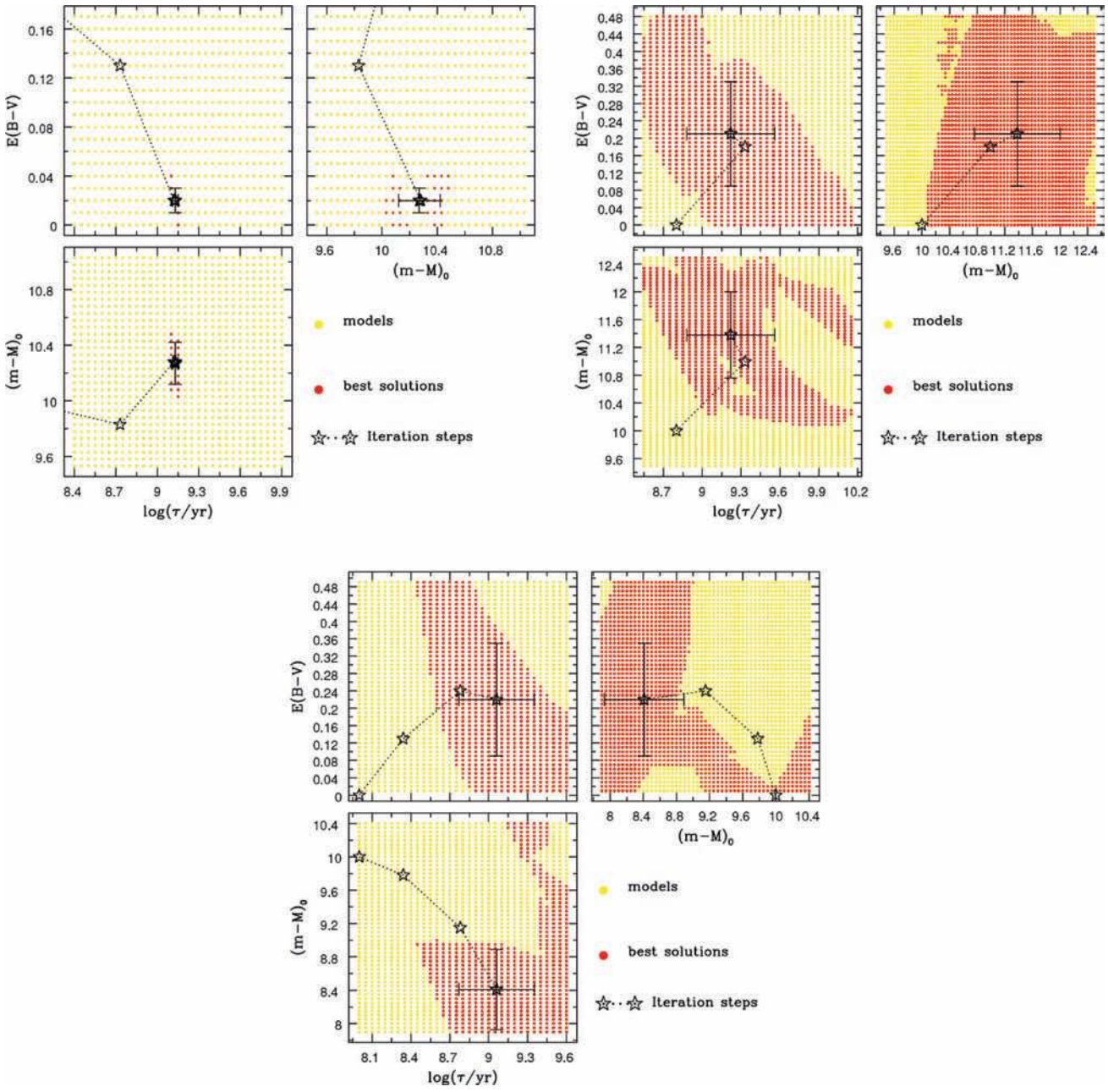

Figure 7. Examples of explored parameter space for NGC 3680 (upper left-hand panel) and NGC 2180 (upper right-hand panel) and Test Field (bottom panels). The evolution of the iteration solution (open stars) is shown.

The fundamental parameters obtained from the present method for NGC 3680 and 2180 are in agreement with the previous studies, considering uncertainties and differences between extracted radii.

The explored parameter spaces for the objects are shown in Fig. 7. These figures present the best solutions and the evolution of an average solution after each iteration. Some trends in the parameter space can be seen. For NGC 3680, the best fits (red points) correspond to a small value set from all tested solutions, especially for $\log(\tau/\mathrm{age})$ versus $(m-M)_0$, where an anticorrelation between these parameters occurs. On the other hand, the panels for the Test Field reveal that the parameter space is filled almost randomly, often distributed in two solution subgroups. For NGC 2180, we have an intermediate behaviour. Although the number of best fits is greater than in NGC 3680, the anticorrelation between $\log(\tau/\mathrm{age})$ and $(m-M)_0$ can be seen.

3.4 Statistical comparison with field stars

The results presented in the previous sections will be meaningful only if one is sure that the number of fitted stars for the POCR cannot be reproduced by the field samples. In other words, one has to check whether there is not a single field sample (equal to the POCR size) with an isochrone fit of the same quality as the POCR. Otherwise, the results cannot be statistically demonstrated.

Adopting this simple principle, an objective criterion to disentangle the POCR from field star background was developed. The first step was to select neighbouring field samples from the surrounding control field (typically 300 $N_{\mathrm{samples,tot}}$ with radius R_{cut}). Different from the random field selection in Section 3.1, the present one sweeps a uniform grid covering the whole surrounding control field area. For each of them, an isochrone fit solution and consequently an n_{fit} value are found, following exactly the same procedure as applied to the POCR (Section 3.3). This approach assures two basic requirements to a reliable field versus POCR comparison: (i) the neighbouring field samples and POCR are undergoing the same treatment; and (ii) the signature of the field fluctuations is impressed in the n_{fit} distribution for the neighbouring field samples. So, using the dispersion ($\sigma_{n_{\mathrm{fit}}}$) in this distribution as well as its 99th and 100th percentile loci, a critical parameter is defined as

$$n_{\mathrm{fit,lim}} = \max(n_{\mathrm{fit,99}} + 1\sigma_{\mathrm{nfit}}, n_{\mathrm{fit,100}})\,. \quad (9)$$

Finally, a POCR is characterized as

$$\text{a non-field fluctuation, if } n_{\mathrm{fit,POCR}} > n_{\mathrm{fit,lim}}; \quad (10)$$

$$\text{a field fluctuation, if } n_{\mathrm{fit,POCR}} < n_{\mathrm{fit,99}}. \quad (11)$$

The statistical comparison with the field is illustrated in Fig. 8, which presents the n_{fit} distribution for the field stars of NGC 3680, NGC 2180 and the Test Field as compared to the $n_{\mathrm{fit,POCR}}$ value for each object. The number of fitted stars for NGC 3680 and 2180 is nowhere reproduced by their neighbouring field samples. On the other hand, as expected, the same figure also reveals that the Test Field $n_{\mathrm{fit,POCR}}$ value is located within the n_{fit} field star distribution. This is also represented by the complex solution pattern in the parameter space (Fig. 7).

In general, a surrounding control field has many faint stars ($14 \leq J \leq 15$ mag). To avoid too much weight for them in the n_{fit} field distributions (Fig. 8), we consider stars with $J \leq 14$ mag.

To guarantee that the comparison between the n_{fit} distribution for the field stars and $n_{\mathrm{fit,POCR}}$ represents a distinct distribution of stars in the CMDs, we checked by eye inspection the set of field CMDs that the tool indicated as most resembling the object CMD. Fig. 9 presents the sample field CMDs.

3.5 Testing the extent of the surrounding control field

The statistics of the field of radius 30 arcmin is not usual in star cluster studies. Studies based on the 2MASS, such as the present one, are allowing to utilize enormous field areas for comparison purposes (Bonatto & Bica 2009a). The relatively high Galactic latitudes where we are working are expected to be stable, in contrast to positions very close to the Galactic plane, where reddening variations may be important. To test the stability of the present diagnostic tool and/or larger field areas, we extended the surrounding control field from radius 30–60 arcmin. We did this for NGC 272 and ESO 324 SC15. The number of small neighbouring field samples for both targets increased from 386 to 999. The results originated from the cut-off radius, star count distribution for field star samples, target and field CMDs, and the parameter spaces are very similar (see the respective panels in Figs A3 and A5). We illustrate the resulting number of isochrone-fitted stars weighted by membership probability for targets and fields within the control field radius of

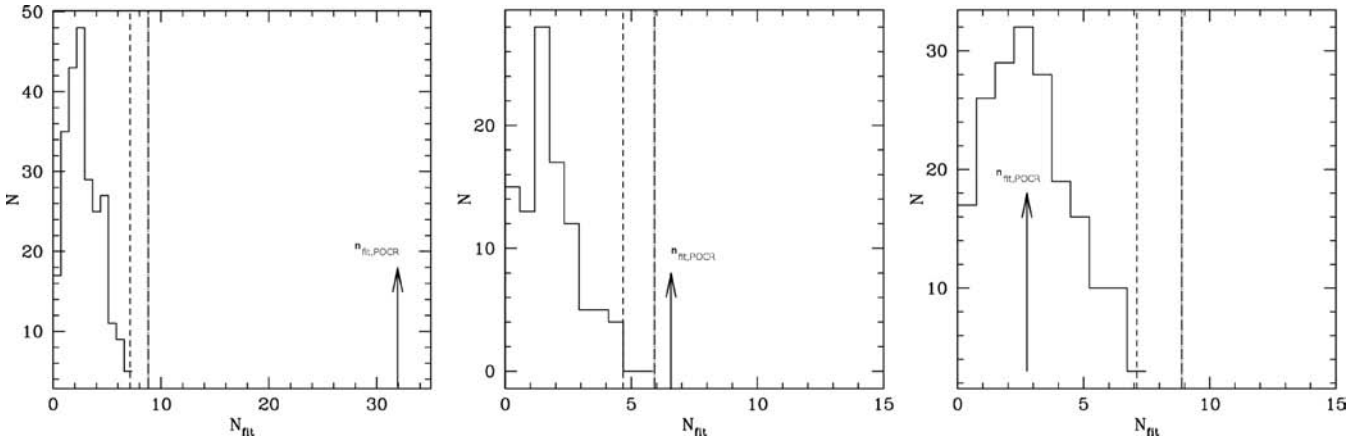

Figure 8. Target and fields: number of isochrone-fitted stars weighted by membership probability. Examples of n_{fit} distributions for the comparison fields (histogram) and the $n_{\mathrm{fit,POCR}}$ (arrow). Left-hand to right-hand panel: NGC 3680, NGC 2180 and Test Field. The percentile locus 99 per cent and $n_{\mathrm{fit,lim}}$ are marked (vertical dashed lines).

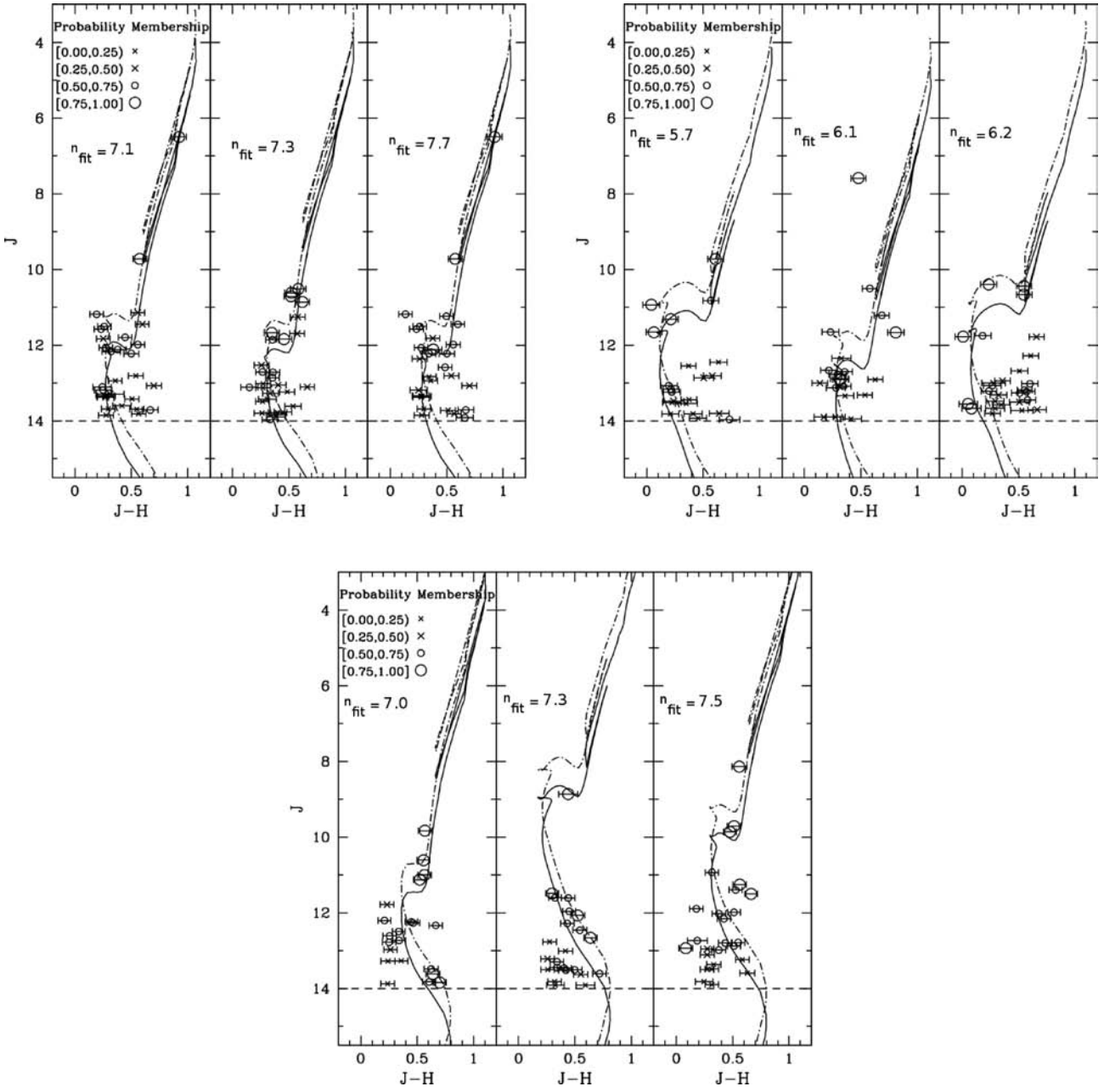

Figure 9. The three comparison fields that resemble most the target CMDs. J versus $(J - H)$ CMDs of comparison fields with $n_{\rm fit}$ comparable with $n_{\rm fit,POCR}$ for NGC 3680 (top left-hand panels), NGC 2180 (top right-hand panels) and Test Field (bottom panels).

60 arcmin in Fig. 10. Comparing with the radius 30 arcmin [panels (g) in Figs A3 and A5), the behaviours are essentially the same.

4 TESTING A POCR NATURE

To distinguish a POCR from its background field, a critical overall analysis of the results obtained from the diagnostic tool is necessary. We illustrate that by: (i) cut-off radius determination (Figs 2 and 3); (ii) the radial density profile construction (Fig. 4); (iii) best isochrone fit (Fig. 6); (iv) mapping the parameter space (Fig. 7); and (v) histogram of the number of isochrone-fitted stars weighted by membership probability ($n_{\rm fit}$) for the comparison fields (Fig. 8).

By comparing results of the reference targets (NGC 3680, NGC 2180 and Test Field) with the POCRs, we established criteria to constrain their nature. A POCR is considered a physical system from the photometric point of view if

(i) there is a significant star density contrast with respect to the field (Section 3.1);

(ii) the radial density profile has at least one peak in the central POCR area;

(iii) an isochrone solution can be found; and

(iv) the POCR CMD must differ from the comparison fields in terms of the number of stars, isochrone fit and/or membership determinations.

The final results for the four POCRs are provided in Table 3, where the numbers of isochrone-fitted stars in the POCR and field can be compared. By columns: (1) designation; (2) average of

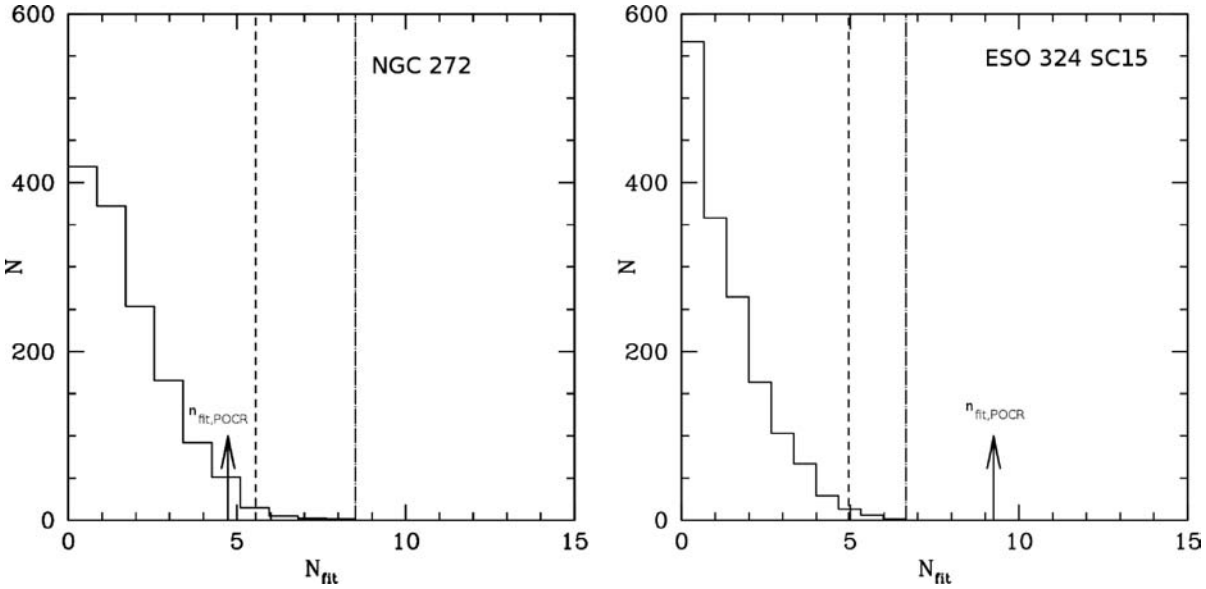

Figure 10. Number of isochrone-fitted stars weighted by membership probability for the neighbouring sample fields ($n_{\rm fit}$ – histogram) and the targets ($n_{\rm fit,POCR}$ – arrow), but for the surrounding control field radius 60 arcmin. The percentile locus 99 per cent and $n_{\rm fit,lim}$ are marked (vertical dashed lines).

Table 3. Number of isochrone-fitted stars for the targets together with the POCR final characterization.

POCR	$\langle n_{\rm fit,field}\rangle$	$\sigma_{\rm nfit,field}$	$n_{\rm fit,99}$	$n_{\rm fit,lim}$	$n_{\rm fit,POCR}$	Results
NGC 3680	2.0	1.7	7.13	8.8	31.3	Open cluster
NGC 2180	1.8	1.2	4.7	5.9	6.6	Evolved open cluster
Test Field	3.0	1.8	7.1	8.9	2.7	Field fluctuation
DoDz 6[a]	0.4	0.6	1.9	2.8	4.7	Field fluctuation
NGC 272	1.8	1.3	5.4	6.7	4.8	Field fluctuation
ESO 435 SC48	1.2	1.0	4.5	4.1	8.6	Cluster remnant[b]
ESO 324 SC15	1.2	1.1	4.7	5.9	9.3	Cluster remnant[b]

[a]Results from solution 1.
[b]OCR according to the photometric analysis.

isochrone-fitted stars ($\langle n_{\rm fit,field}\rangle$) and (3) standard deviation ($\sigma_{\rm nfit,field}$) for the comparison fields; (4), (5) and (6) number of isochrone-fitted stars in the percentile position 99 ($n_{\rm fit,99}$), in the limiting value ($n_{\rm fit,lim}$ – Section 3.4) and in the POCR area ($n_{\rm fit,POCR}$), respectively; and (7) results.

Comparing columns (3) and (5) of Table 3 for the reference targets with the POCRs ESO 435 SC48 and ESO 324 SC15, one concludes that the latter appears to be physical systems, as long as the photometric data are concerned. On the same grounds, NGC 272 is a field fluctuation. The DoDz 6 results are not conclusive from Table 3. However, the scattering observed in the space parameter (panels A1 and A2) points to a field fluctuation.

We present five postscript plots in Appendix A with complete sets of results for each POCR. They are essential for the interpretation of their nature. According to the criteria and plots, the POCRs can be described as follows:

DoDz 6: despite the fact that there are five bright stars in the POCR direction and not in the comparison fields, these stars are probably not physically related and represent an asterism. Figs A1 and A2 show that the stellar distribution in the CMD allows at least two sets of isochrone solutions: (i) solution 1 – $\log(\tau/{\rm yr}) = 7.49 \pm 0.39$, $(m-M)_0 = 6.56 \pm 0.06$, $E(B-V) = 0.09 \pm 0.06$ and (ii) solution 2 – $\log(\tau/{\rm yr}) = 8.14 \pm 0.45$, $(m-M)_0 = 6.49 \pm 0.26$, $E(B-V) = 0.11 \pm 0.06$.

NGC 272: it was characterized as a field fluctuation because there occur comparison fields with the same stellar density as the object. Moreover, there are comparison fields that fit better their CMDs than the POCR itself [see panels (a)–(e) of Fig. A3]. The $n_{\rm fit}$ value for NGC 272 falls in the $n_{\rm fit}$ field distribution [panel (g) of Fig. A3], supporting the latter conclusion.

ESO 435 SC48: we concluded that it is a probable physical system. The space parameter [panel (f) of Fig. A4] shows the same anticorrelation between $\log(\tau/{\rm age})$ and $(m-M)_0$ as identified for NGC 3680 (Fig. 7). The POCR fundamental parameters are $\log(\tau/{\rm age}) = 9.30 \pm 0.17$ that correspond to an age of $1.9^{+0.9}_{-0.3}$ Gyr, a reddening value of $E(B-V) = 0.09 \pm 0.06$, a distance to the Sun $d_\odot = 0.83 \pm 0.09$ kpc, a height from the plane $z = 0.32 \pm 0.03$ kpc and Galactocentric distance $R_{\rm GC} = 8.1 \pm 0.1$ kpc (using a distance of the Sun to the Galactic Centre $R_{\rm GC} = 7.2$ kpc, Bica et al. 2006).

ESO 324 SC15: probable physical system. Panel (f) of Fig. A5 also shows the same anticorrelation as observed in NGC 3680 (Fig. 7). The POCR fundamental parameters are: $\log(\tau/{\rm age}) = 9.02 \pm 0.12$, corresponding to an age of $1.0^{+0.4}_{-0.3}$ Gyr, $E(B-V) = 0.13 \pm 0.07$, $d_\odot = 0.94 \pm 0.15$ kpc, z = 0.33 ± 0.05 kpc and $R_{\rm GC} = 7.5 \pm 0.8$ kpc.

Table 4 presents stars within $R_{\rm cut}$ for each POCR. By columns: (1) POCR; (2) and (3) J2000.0 equatorial coordinates; (4), (5) and (6) 2MASS magnitudes and colour uncertainties, respectively; (7)

Table 4. POCR stars within the cut radius (R_{cut}). Note: since DoDz 6 and NGC 272 resulted field fluctuations, the stars in column (8) are non-members.

Designation	α (J2000) (°)	δ (J2000) (°)	$(J-H)$ (mag)	J (mag)	$\sigma_{(J_H)}$ (mag)	Probability	Membership[a]
DoDz 6	251.34716	38.33194	0.604	7.587	0.025	0.990	–
DoDz 6	251.34150	38.34671	0.195	8.375	0.030	0.979	–
DoDz 6	251.36949	38.35571	0.516	8.618	0.033	0.995	–
DoDz 6	251.38154	38.37324	0.379	9.727	0.030	0.969	–
DoDz 6	251.38152	38.36624	0.533	10.324	0.024	0.938	–
DoDz 6	251.31711	38.32593	0.579	11.659	0.030	0.702	–
DoDz 6	251.35536	38.32343	0.470	14.166	0.037	0.496	–
DoDz 6	251.33604	38.37743	0.395	14.302	0.040	0.553	–
DoDz 6	251.40855	38.34068	0.650	14.681	0.045	0.593	–
DoDz 6	251.33265	38.37256	0.652	14.719	0.044	0.566	–
DoDz 6	251.32923	38.30732	0.614	13.754	0.031	0.000	–
DoDz 6	251.32188	38.32847	0.480	14.760	0.052	0.331	–
DoDz 6	251.29891	38.36828	0.730	14.773	0.045	0.576	–
DoDz 6	251.34001	38.31133	0.726	14.882	0.044	0.679	–
NGC 272	12.82584	35.84765	0.165	8.553	0.028	0.969	–
NGC 272	12.84214	35.81994	0.446	9.594	0.030	0.969	–
NGC 272	12.85409	35.80954	0.275	10.842	0.029	0.897	–
NGC 272	12.84839	35.87445	0.422	11.096	0.029	0.794	–
NGC 272	12.86650	35.81173	0.283	11.885	0.030	0.887	–
NGC 272	12.81838	35.85640	0.290	12.074	0.029	0.928	–
NGC 272	12.85539	35.81170	0.292	12.826	0.038	0.547	–
NGC 272	12.86034	35.82765	0.644	13.508	0.033	0.551	–
NGC 272	12.87390	35.82925	0.588	13.567	0.032	0.537	–
NGC 272	12.79377	35.88988	0.382	13.592	0.031	0.033	–
NGC 272	12.82481	35.79962	0.345	13.932	0.039	0.434	–
NGC 272	12.77379	35.82101	0.398	14.022	0.042	0.331	–
NGC 272	12.78633	35.81352	0.567	14.126	0.039	0.379	–
NGC 272	12.85903	35.81298	0.735	14.583	0.042	0.000	–
NGC 272	12.82604	35.81733	0.653	14.626	0.052	0.000	–
ESO 435 SC48	152.38330	−28.36200	0.469	10.263	0.033	0.950	pm
ESO 435 SC48	152.42150	−28.36376	0.263	11.207	0.033	0.914	pm
ESO 435 SC48	152.40042	−28.35490	0.236	11.894	0.034	0.955	pm
ESO 435 SC48	152.41734	−28.37949	0.337	12.102	0.034	0.905	pm
ESO 435 SC48	152.39390	−28.32513	0.257	12.485	0.034	0.851	pm
ESO 435 SC48	152.37559	−28.36562	0.383	12.756	0.033	0.821	pm
ESO 435 SC48	152.37378	−28.36246	0.302	12.829	0.033	0.855	pm
ESO 435 SC48	152.36852	−28.34117	0.485	13.168	0.034	0.529	pm
ESO 435 SC48	152.41342	−28.36144	0.337	13.562	0.033	0.543	pm
ESO 435 SC48	152.36602	−28.35340	0.477	13.710	0.041	0.759	pm
ESO 435 SC48	152.39747	−28.37592	0.537	13.877	0.034	0.534	pm
ESO 435 SC48	152.38509	−28.35042	0.260	14.545	0.043	0.385	pnm
ESO 324 SC15	200.86967	−41.87476	0.679	9.382	0.057	0.986	pm
ESO 324 SC15	200.92343	−41.89363	0.210	9.661	0.031	0.991	pm
ESO 324 SC15	200.87888	−41.88707	0.334	9.895	0.034	0.998	pm
ESO 324 SC15	200.90377	−41.90871	0.158	11.137	0.030	0.982	pm
ESO 324 SC15	200.90774	−41.87865	0.209	11.845	0.030	0.966	pm
ESO 324 SC15	200.92283	−41.86874	0.604	11.597	0.031	0.864	lpm
ESO 324 SC15	200.90065	−41.89375	0.225	11.923	0.031	0.950	pm
ESO 324 SC15	200.93950	−41.87688	0.277	12.290	0.033	0.896	pm
ESO 324 SC15	200.87897	−41.89088	0.322	12.298	0.031	0.880	pm
ESO 324 SC15	200.90749	−41.87268	0.317	12.741	0.031	0.830	pm
ESO 324 SC15	200.94612	−41.88042	0.358	12.865	0.033	0.812	pm
ESO 324 SC15	200.89125	−41.85468	0.428	13.738	0.045	0.477	lpm
ESO 324 SC15	200.89249	−41.88569	0.483	13.751	0.042	0.455	lpm
ESO 324 SC15	200.91294	−41.86008	0.486	14.059	0.034	0.000	pnm
ESO 324 SC15	200.86105	−41.88567	0.335	14.492	0.043	0.403	pnm
ESO 324 SC15	200.91155	−41.89926	0.587	14.604	0.059	0.220	lpm
ESO 324 SC15	200.91421	−41.91381	0.339	14.688	0.041	0.260	pnm

[a] 'pm' means a probable member; 'lpm' means a less-probable member; and 'pnm' means a probable non-member.

probability; and (8) membership. For DoDz 6 and NGC 272, characterized as field fluctuations, no membership is provided. Each star was classified as: (i) a probable member if a membership probability value is $\geq$50 per cent and it is compatible with the isochrone (single and binaries); (ii) a less-probable member if it reaches $\geq$50 per cent, but is compatible with the isochrone; (iii) a less-probable member reaching $\leq$50 per cent, but is compatible with the isochrone; and (iv) a probable non-member if it reaches $\leq$50 per cent and it is not compatible with the isochrone.

5 DISCUSSION AND CONCLUDING REMARKS

Based on Platais et al. (1998)'s photometric criterion (Section 1) to distinguish physical stellar groups and field fluctuations, we developed a diagnostic tool to study CMDs of POCRs using 2MASS data. We analysed four POCRs by comparing them with the open cluster NGC 3680, the evolved open cluster NGC 2180 and a Test Field, all located at relatively high Galactic latitudes. We performed analyses to test their physical nature, and to determine ages, distances and reddening values in a self-consistent way. Two POCRs (ESO 435 SC48 and ESO 324 SC15) appear to be physical stellar systems.

The algorithm compares statistically the CMD distribution of a poorly populated star concentration and a series of comparison fields surrounding it. The method takes into account star densities, membership probabilities and a set of isochrones. As an eye check, we inspect the target CMD and the three comparison fields that most resemble it. They must be dissimilar. We intended to use the maximal information stocked in the CMD distributions.

This study gave directions on how to analyse poorly populated stellar concentrations. A meaningful analysis of a POCR requires field decontamination. A star count above the average background field value does not guarantee the physical status of a POCR, because the membership attribution may result unfavourable, among other reasons. We must be careful with the cut-off radius of the target. Extractions in exceedingly large areas can dilute the results of a physical group. Using the parameter space, we can verify whether the solution space is concentrated or spread. In the case of DoDz 6, the spread of solutions is prohibitive, so that the available photometric data characterized it as a field fluctuation. On the other hand, ESO 324 SC15 and ESO 435 SC48 have a compact solution distribution. The latter behaviour is that expected for more populated stellar concentrations, such as open clusters.

Open cluster catalogues include a number of poorly populated concentrations. The present tool was optimized to photometrically deal with these targets and to select POCR candidates for future kinematical and chemical composition studies. The purpose of this paper is to introduce the method together with some test targets. In upcoming studies, we intend to explore larger target samples to disentangle POCRs and OCRs, in order to determine their photometric characterization.

ACKNOWLEDGMENTS

We thank the anonymous referee for interesting remarks. We acknowledge support from the Brazilian Institutions FAPESP, Capes and CNPq. This work makes use of data products from the 2MASS, which is a joint project of the University of Massachusetts and Infrared Processing and Analysis/California Institute of Technology, funded by the National Aeronautics and Space Administration and the National Science Foundation. This research has also made use of the WEBDA data base operated at the Institute for Astronomy of the University of Vienna.

REFERENCES

Bica E., Santiago B. X., Dutra C. M., Dottori H., de Oliveira M. R., Pavani D., 2001, A&A, 366, 827
Bica E., Bonatto C., Barbuy B., Ortolani S., 2006, A&A, 450, 105
Bonatto C., Bica E., 2007, MNRAS, 377, 1301
Bonatto C., Bica E., 2009a, MNRAS, 392, 483
Bonatto C., Bica E., 2009b, MNRAS, 397, 1915
Bonatto C., Bica E., Pavani D. B., 2004, A&A, 427, 485
Davenport J. R. A., Sandquist E. L., 2010, ApJ, 711, 559
de la Fuente Marcos R., 1997, A&A, 322, 764
Dias W. S., Alessi B. S., Moitinho A., Lépine J. R. D., 2002, A&A, 389, 871
Friel E. D., 1995, ARA&A, 33, 381
Froebrich D., Scholz A., Raftery C. L., 2007, MNRAS, 374, 399
Girardi L., Bertelli G., Bressan A., Chiosi C., Groenewegen M. A. T., Marigo P., Salasnich B., Weiss A., 2002, A&A, 391, 195
Ivanov V. D., Borissova J., Pessev P., Ivanov G. R., Kurtev R., 2002, A&A, 394, L1
Kerber L. O., Santiago B. X., 2005, A&A, 435, 77
Kerber L. O., Santiago B. X., Castro R., Valls-Gabaud D., 2002, A&A, 390, 121
Kharchenko N. V., Piskunov A. E., Röser S., Schilbach E., Scholz R.-D., 2005, A&A, 438, 1163
Kruijssen J. M. D., 2009, A&A, 507, 1409
Mercer E. P. et al., 2005, ApJ, 635, 560
Mermilliod J.-C., Paunzen E., 2003, A&A, 410, 511
Mighell K. J., Rich R. M., Shara M., Fall S. M., 1996, AJ, 111, 2314
Monteiro H., Dias W. S., Caetano T. C., 2010, A&A, 516, A2
Ochsenbein F., Bauer P., Marcout J., 2000, A&AS, 143, 23
Oort J. H., 1958, RA, 5, 507
Pavani D. B., Bica E., 2007, A&A, 468, 139
Pavani D. B., Bica E., Dutra C. M., Dottori H., Santiago B. X., Carranza G., Díaz R. J., 2001, A&A, 374, 554
Pavani D. B., Bica E., Ahumada A. V., Clariá J. J., 2003, A&A, 399, 113
Platais I., Kozhurina-Platais V., van Leeuwen F., 1998, AJ, 116, 2423
Reylé C., Robin A. C., 2002, A&A, 384, 403
Schlegel D. J., Finkbeiner D. P., Davis M., 1998, ApJ, 500, 525
Skrutskie M. F. et al., 2006, AJ, 131, 1163
Soares J. B., Bica E., 2002, A&A, 388, 172

APPENDIX A: POSTSCRIPT FIGURE OF THE TARGETS

The plots in each panel show the complete output figures for the targets: (a) determination of the largest radius that maximizes the percentile position as in Fig. 2; (b) $n_{\rm field}$ histogram as in Fig. 3; (c) radial stellar density profile as in Fig. 4; (d) and (e) CMDs following Figs 5 and 9, respectively; (f) parameter space as in Fig. 7; (g) $n_{\rm fit}$ histogram as in Fig. 8; and (h) DSS image with $R = 2R_{\rm cut}$.

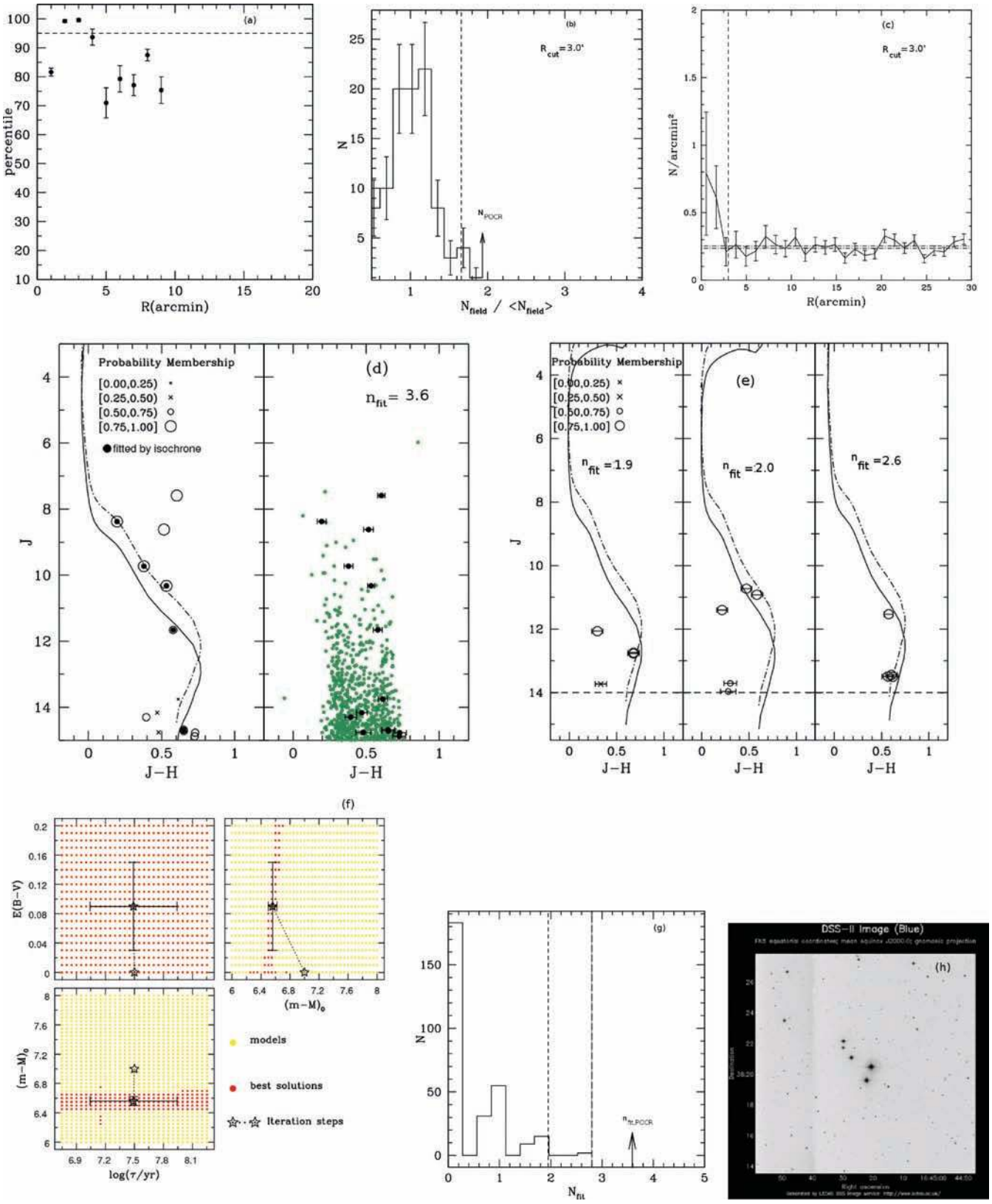

Figure A1. Target panel for DoDz 6 solution 1.

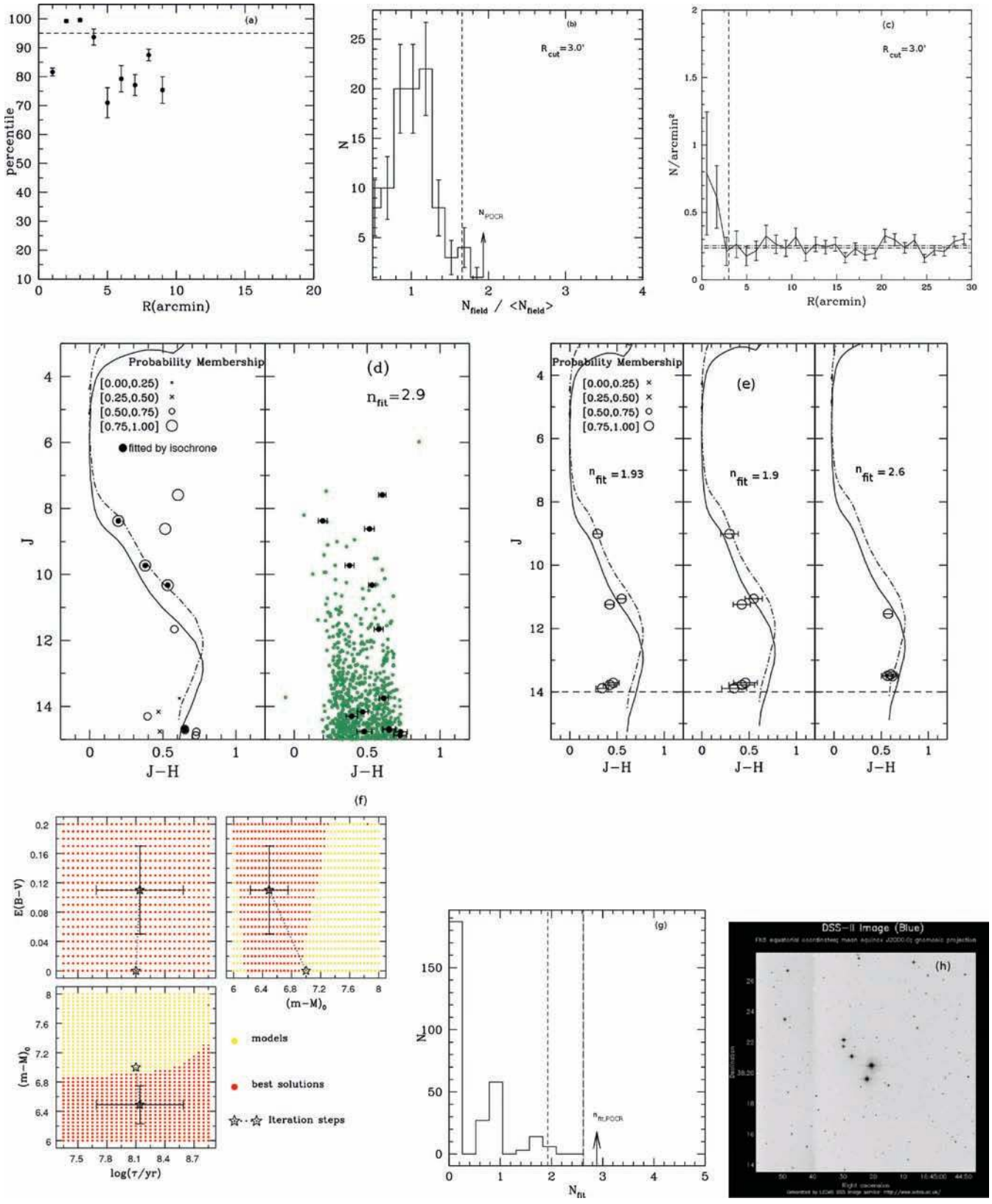

Figure A2. Target panel for DoDz 6 solution 2.

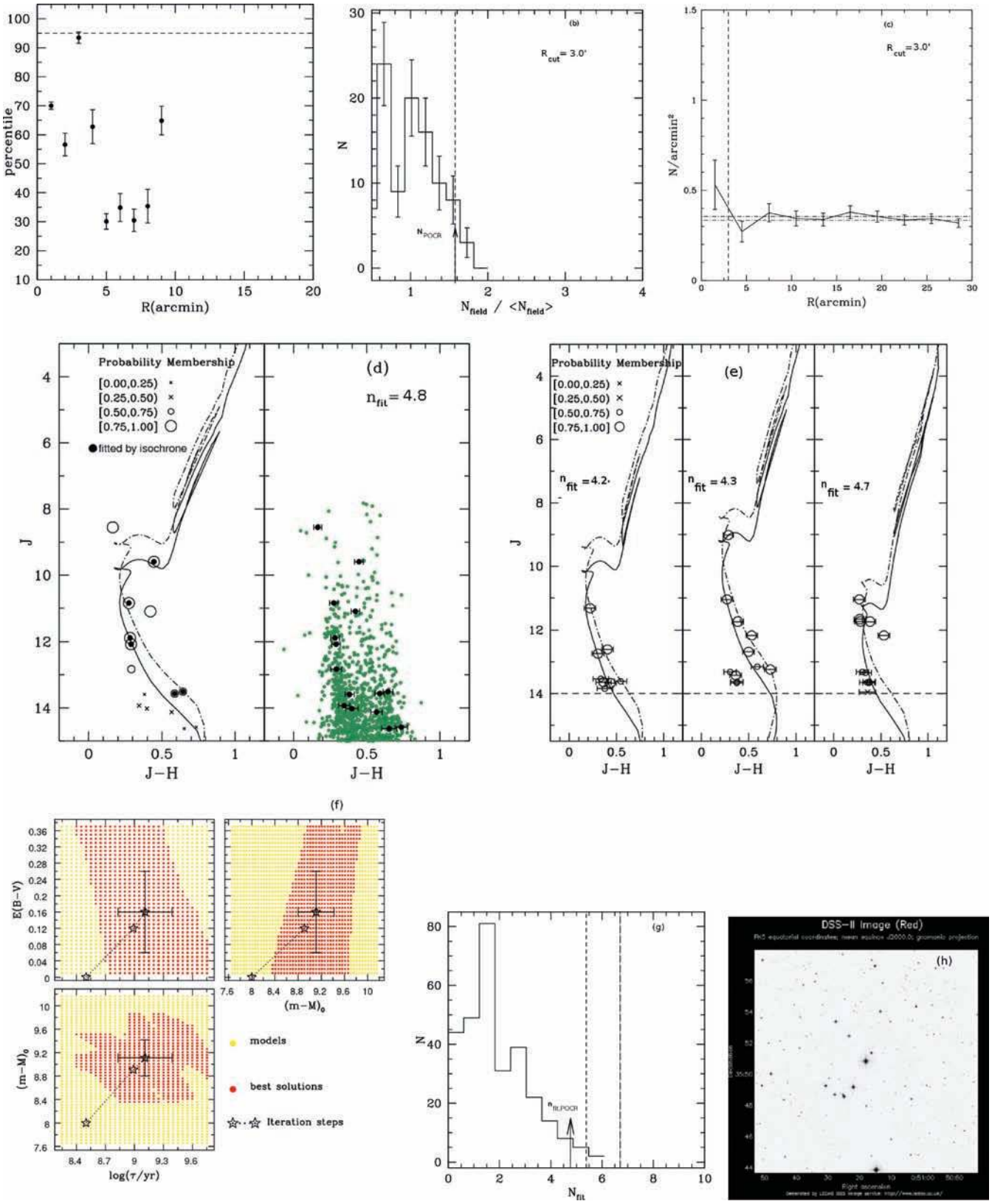

Figure A3. Same as Fig. A1, but for NGC 272.

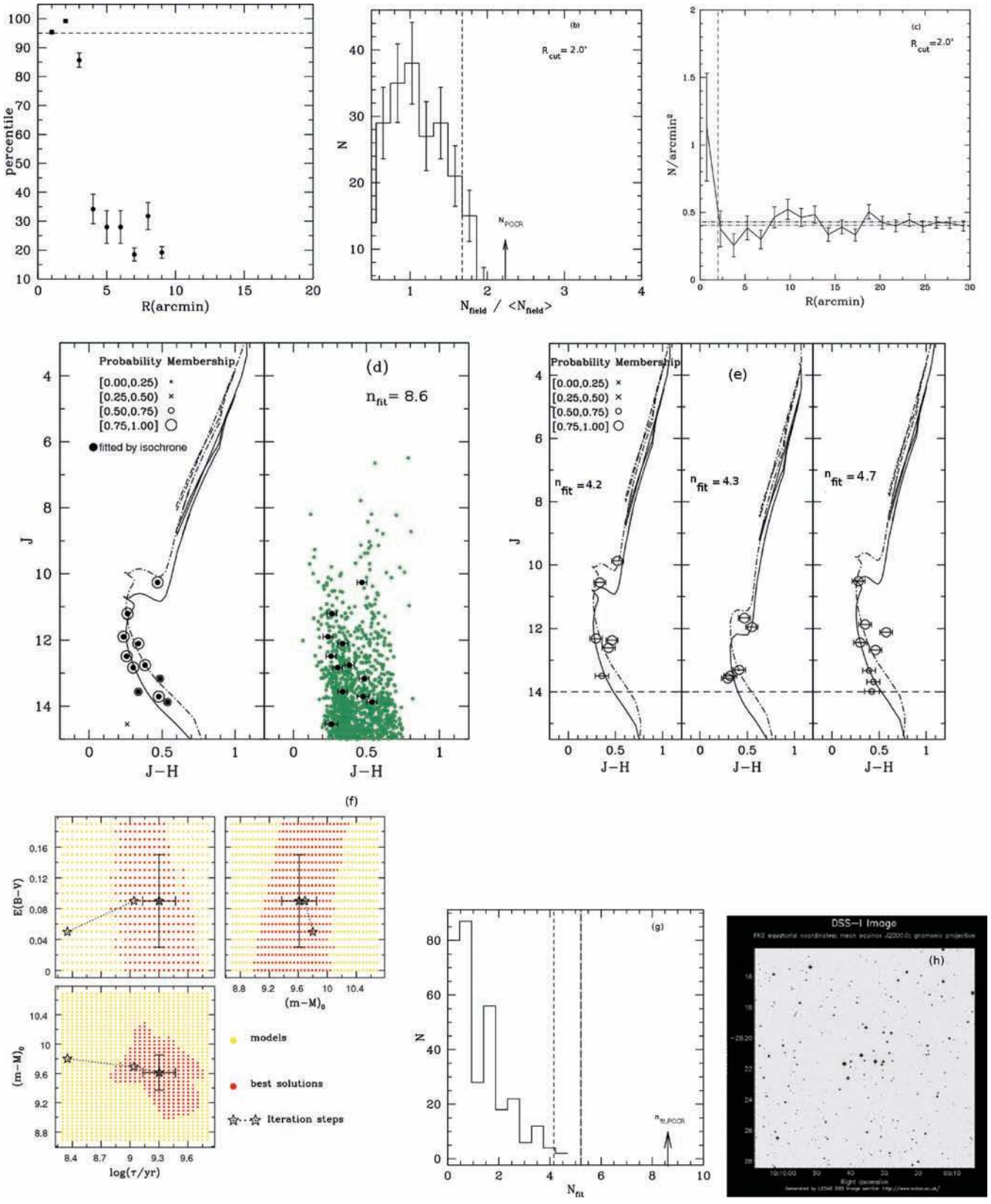

Figure A4. Same as Fig. A1, but for ESO 435 SC48.

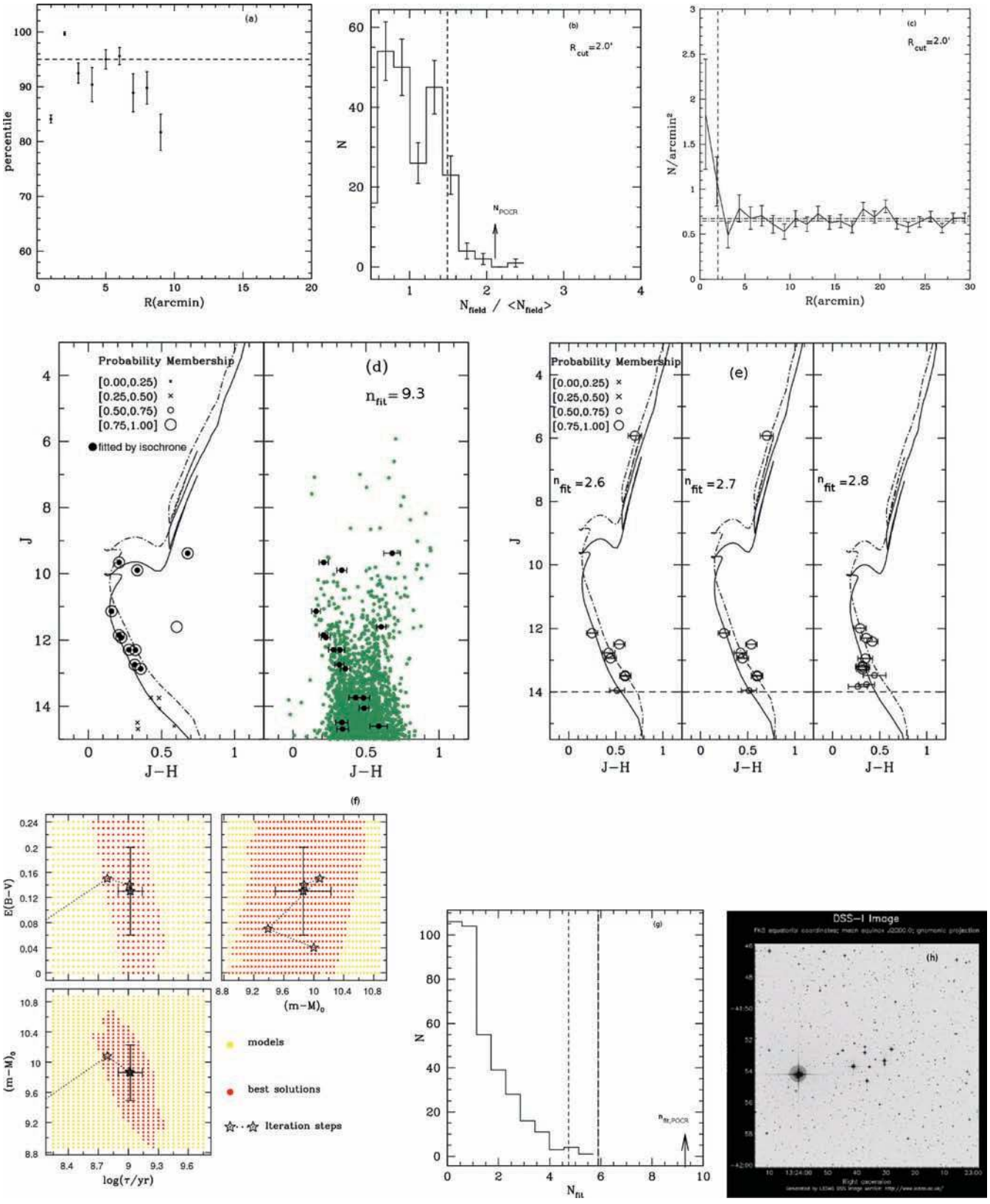

Figure A5. Same as Fig. A1, but for ESO 324 SC15.

This paper has been typeset from a TEX/LATEX file prepared by the author.